Monthly Notices of the ROYAL ASTRONOMICAL SOCIETY

MNRAS **544,** L167–L173 (2025) https://doi.org/10.1093/mnrasl/slaf116
Advance Access publication 2025 November 11

Ruling out dominant electron scattering in Little Red Dots' Rosetta Stone using multiple hydrogen lines

Matilde Brazzini [1,2,3,4★] Francesco D'Eugenio [1,2★] Roberto Maiolino,[1,2,5] Ignas Juodžbalis,[1,2] Xihan Ji [1,2] Jan Scholtz[1,2] and Seok-Jun Chang [6]

[1]*Kavli Institute for Cosmology, University of Cambridge, Madingley Road, Cambridge CB3 0HA, UK*
[2]*Cavendish Laboratory – Department of Physics, University of Cambridge, 19 JJ Thomson Avenue, Cambridge CB3 0HE, UK*
[3]*Department of Physics, Astronomy Section, University of Trieste, Via G.B. Tiepolo 11, I-34143 Trieste, Italy*
[4]*INAF – Osservatorio Astronomico di Trieste, Via G.B. Tiepolo 11, I-34143 Trieste, Italy*
[5]*Department of Physics and Astronomy, University College London, Gower Street, London WC1E 6BT, UK*
[6]*Max-Planck-Institut für Astrophysik, Karl-Schwarzschild-Straße 1, D-85748 Garching bei München, Germany*

Accepted 2025 November 3. Received 2025 October 23; in original form 2025 July 15

ABSTRACT

Most little red dots (LRDs) hosting active galactic nuclei (AGNs) show broad Hα emission, which recent studies ascribe to scattering off free electrons within an ionized medium embedding the broad-line region (BLR), rather than directly from the BLR itself. If correct, this model would imply intrinsically narrower broad line widths, leading to black hole masses that are up to two orders of magnitude smaller than what is inferred when assuming that the whole broad line emission comes from the BLR. To test this, we present a joint analysis of multiple hydrogen recombination lines in the 'Rosetta Stone' AGNs, the brightest known LRD at $z = 2.26$. We show that Hα, Hβ, and Paβ have different spectral profiles, which is inconsistent with the predictions of the simple scattering scenario. Additionally, we test a variety of exponential models and show that none of them can simultaneously reproduce all three line profiles with physically plausible parameters. The inadequacy of these models for the Rosetta Stone implies that the scenario of electron scattering by an ionized medium embedding the BLR is not universally applicable to LRDs and AGNs, and therefore provides a counterexample to the claim of a universal and systematic overestimation of black hole masses.

Key words: galaxies: active – galaxies: high-redshift – quasars: supermassive black holes.

1 INTRODUCTION

James Webb Space Telescope (*JWST*) has revolutionized our understanding of supermassive black hole formation and evolution in the early Universe, revealing a new population of low-mass, low-luminosity active galactic nuclei (AGNs; Y. Harikane et al. 2023; D. D. Kocevski et al. 2023; R. Maiolino et al. 2024; J. Matthee et al. 2024; I. Juodžbalis et al. 2025a). These sources are usually compact and weak in both X-rays and radio emission (G. Mazzolari et al. 2024, 2025; R. Maiolino et al. 2025), leading to initial scepticism regarding their AGN nature. However, their classification is now firmly established through their time variability (L. J. Furtak et al. 2025; X. Ji et al. 2025a) and the detection of broad Hα emission [full width at half-maximum (FWHM) $\gtrsim 1000\,\mathrm{km\,s^{-1}}$] with no broad counterpart in [O III] $\lambda\lambda$4959, 5007, ruling out outflows and confirming that broad Hα originates from the broad-line region (BLR). A fraction of these AGNs (ranging from 10–30 per cent, K. N. Hainline et al. 2025, to ∼44 per cent, Z. Zhang et al. 2025) further exhibit unusual properties compared to standard type I, including a characteristic 'v'-shaped ultraviolet-to-optical spectral energy distribution (SED) and a prominent spectral break at rest-frame wavelength ∼3700 Å (i.e. the Balmer break). These sources have been dubbed little red dots (LRDs).

The discovery of LRDs has raised more questions than current observations can answer. In particular, an increasing number of high-redshift LRDs exhibit deep Balmer and He I λ10829 absorption features (I. Juodžbalis et al. 2024; J. Matthee et al. 2024; F. D'Eugenio et al. 2025a, 2025b; X. Ji et al. 2025a; F. Loiacono et al. 2025; B. Wang et al. 2025), whose physical origin remains uncertain. One plausible explanation invokes absorption by extremely dense gas embedding the BLR ($n_\mathrm{H} \gtrsim 10^9$ cm^{-3}; K. Inayoshi & R. Maiolino 2025). If this interpretation is correct, the presence of such high-density gas could also account for the X-ray weakness of these sources – assuming they are Compton thick – and also for their prominent Balmer break, ruling out its stellar origin (I. Labbe et al. 2024). Moreover, if the medium is ionized, it is possible that the observed broad emission-line widths may arise from electron scattering within this gaseous envelope, rather than from bulk gas motion in the BLR itself. This hypothesis, first tested by V. Rusakov et al. (2025, hereafter R25), suggests that the intrinsic width of the broad lines could be 5–10 times narrower than currently measured, potentially leading to systematic overestimates of black hole masses by up to two orders of magnitude. In particular, R25 studied

★ E-mail: matilde.brazzini@inaf.it (MB); fd391@cam.ac.uk (FD)

the Hα line profile in a sample of 13 *JWST*-discovered AGN at $z \sim 3$–7 assuming a narrow Gaussian component, a broad Gaussian component representing the unscattered light from the BLR, and an exponential component accounting for the scattered light. They compare the retrieved exponential profiles with a single-Gaussian broad-line model, and find that the former is statistically preferred for all but one of the sources in their sample. In this Letter, we aim to further explore the electron scattering scenario by studying the broad line profiles of multiple hydrogen recombination lines in a luminous LRD at cosmic noon, GN-28074, that, given its brightness and prominent emission and absorption features, has been considered the Rosetta Stone of Little Red Dots (I. Juodžbalis et al. 2024). Our specific target is presented in Section 2, and its peculiar line emission is modelled in Section 3. We discuss our results in Section 4, and draw our conclusions in Section 5. Throughout this work, we assume a flat ΛCDM (Λ cold dark matter) cosmology from Planck Collaboration VI (2020).

2 TARGET AND DATA

GN-28074 is a broad-line AGN at $z = 2.26$ in the GOODS-N (Great Observatories Origins Deep Survey North) field (RA = 189.06458°, Dec. = 62.2738°), observed with *JWST* as part of the *JWST* Advanced Deep Extragalactic Survey (JADES; D. J. Eisenstein et al. 2023, Program ID 1181). The AGN has bolometric luminosity of $\log(L_{\rm bol}) = 45.76$ (I. Juodžbalis et al. 2025a). Undetected in X-rays, it has currently the lowest X-ray to bolometric emission ratio among high-z AGNs ($L_{\rm X}/L_{\rm bol} < 10^{-4}$), three orders of magnitude lower than what is observed in local AGN of similar luminosity (R. Maiolino et al. 2025). It displays the characteristic features of LRDs listed above: a 'v'-shaped SED, broad lines, a Balmer break, and is spatially unresolved at red wavelengths. It also shows deep blueshifted absorption in Hα, Hβ, and He I (I. Juodžbalis et al. 2024). All these features make GN-28074 the ideal object to test the electron scattering scenario, especially given its brightness and redshift, which allow Hα, Hβ, and Paβ lines to be simultaneously observed by *JWST* at high signal-to-noise ratio (SNR). We note that Paγ is also within the observed spectral range, but we neglect it in the following analysis due to strong blending with the metastable He I line. In this Letter, we focus on the medium-resolution spectroscopy ($R = 700$–1500), obtained with 1.7 h of exposure using the NIRSpec (P. Jakobsen et al. 2022) microshutter assembly (P. Ferruit et al. 2022). These data have been processed following the JADES data reduction pipeline (A. J. Bunker et al. 2024; F. D'Eugenio et al. 2025c), with additional updates described in I. Juodžbalis et al. (2024).

3 EMISSION LINE PROFILES

The electron scattering scenario assumes that the BLR is embedded in a dense and ionized medium, where scattering from free electrons produces exponential wings in the emission lines. Since electron scattering is wavelength independent over the spectral range considered in this Letter, all lines from the BLR should be scattered in the same profile. In Fig. 1, we compare (in logarithmic scale) Hα, Hβ, and Paβ profiles, normalized to the red wing of the line at 500 km s^{-1}. Varying the velocity normalization from +500 km s^{-1} to +1500 km s^{-1}, or even −1500 km s^{-1} on the blue side, does not remove the discrepancies in line shapes, challenging electron scattering as the dominant mechanism for line broadening. To investigate this further, we fit emission line profiles using a variety of models, as detailed below. Line fitting is performed within a Bayesian

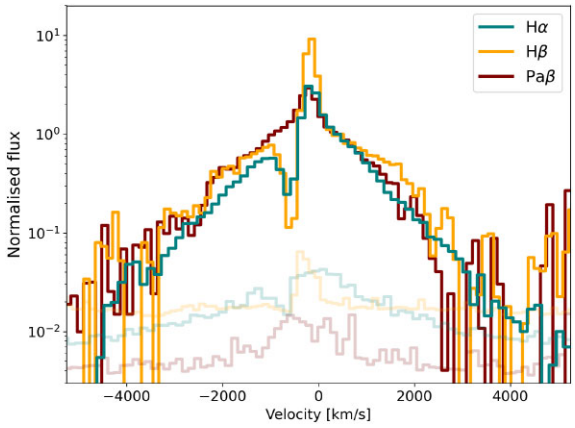

Figure 1. Line profile comparison in velocity space and on logarithmic scale for Hα, Hβ, and Paβ. Their fluxes are normalized to the red 500 km s^{-1}. Spectral errors are reported in lighter colours.

framework, adopting flat, non-informative priors unless otherwise specified. Posterior probability distributions of all parameters are estimated using the Markov chain Monte Carlo integrator EMCEE (D. Foreman-Mackey et al. 2013), initializing the chains near the least-squares solution from the SCIPY's CURVE_FIT function.

We model the local continuum around each emission line with a linear function. Each hydrogen line is fitted with three Gaussians plus an exponential, representing, respectively, the narrow component, an outflow (seen in [O III]), the broad unscattered, and the broad scattered emission from the BLR. The narrow components are forced to have the same intrinsic width, while no constraints are imposed between the broad components. We allow a subpixel velocity offset of ±100 km s^{-1} between the three narrow hydrogen lines, to accommodate possible wavelength calibration issues between the different NIRSpec gratings (F. D'Eugenio et al. 2025c), and an additional velocity shift between the narrow and broad components in the range ±500 km s^{-1}. The velocity and velocity dispersion of the outflow Gaussian components are fixed to those of [O III], which is fitted separately (see Appendix A). We impose the line widths to vary, respectively, between 0 and 700 km s^{-1} for the narrow, and 1000 and 10 000 km s^{-1} for the broad components.

Because the spectral resolution is insufficient to disentangle narrow and outflow components in the [N II] doublet, each nitrogen line is fitted with a single Gaussian sharing the [O III] outflow velocity, with width free to vary within the corresponding [O III] range, as justified by statistical tests.

Lastly, the exponential term representing the scattered light from the BLR is modelled by convolving the BLR Gaussian profile, $G_{\rm BLR}(\lambda)$, with a symmetric exponential (A. Laor 2006) in the form

$$E(\lambda_0, W; \lambda) \propto e^{-\frac{|\lambda-\lambda_0|}{W}}, \quad (1)$$

where λ_0 is the central wavelength (assumed to be the same as the Gaussian BLR), and W is the exponential width, which is allowed to vary in the range 500–10 000 km s^{-1}. The full BLR emission for each line is therefore given by

$$f_{\rm scatt} E(\lambda)\, G_{\rm BLR}(\lambda) + (1 - f_{\rm scatt}) G_{\rm BLR}(\lambda), \quad (2)$$

where $f_{\rm scatt}$ is the fraction of scattered light. We allow W and $f_{\rm scatt}$ to vary independently between the three hydrogen lines.

Balmer absorption is modelled using a standard attenuation model (I. Juodžbalis et al. 2024; F. D'Eugenio et al. 2025c):

$$I(\lambda)/I_0(\lambda) = 1 - C_{\rm f}(1 - e^{-\tau(\lambda)}), \quad (3)$$

where $I_0(\lambda)$ is the spectral flux density before absorption, C_f is the covering factor of the absorber, and $\tau(\lambda)$ is the optical depth profile, assumed to be Gaussian. During the fit, we force the two Balmer absorbers to have the same C_f and kinematics. $I_0(\lambda)$ comprises the continuum and BLR emission, including both the unscattered Gaussian and the scattered exponential terms. Absorbing the continuum is justified by the observation of variable optical continuum in LRDs (X. Ji et al. 2025a), consistent with direct or reprocessed light from the accretion disc. Additionally, absorbing the BLR emission is necessary to avoid unphysical negative fluxes of the absorption when considering only the continuum affected by the absorption (I. Juodžbalis et al. 2024). This physical model implies that the absorbing medium must be located within or just outside the BLR. All line widths are convolved with the instrument line spread function (P. Jakobsen et al. 2022), corrected by a multiplicative factor of 0.7 to take into account slit underfill (e.g. J. E. Greene et al. 2024).

As a first step, we carry out the [O III] line fit to characterize the outflow component. This step is crucial as the bright BLR emission prevents us from reliably decomposing the outflow properties from the Balmer lines. In a successive step, we confirmed that including an outflow component in the hydrogen lines is necessary, as models without it are statistically disfavoured [ΔBIC (Bayesian information criterion) = 25]. We then fit the Hα line individually, and verify that the exponential model performs significantly better than the single-Gaussian model (ΔBIC = 2235, in agreement with R25) and even the double-Gaussian model (ΔBIC = 72). Finally, we carry out the simultaneous fit of Hα, Hβ, and Paβ, assuming the baseline exponential model as presented above. During the fits, we mask spectral regions potentially contaminated by He I $\lambda\lambda$4921, 5017, 6678 and [Fe II] lines, the list of which is constructed by combining those reported in X. Ji et al. (2025b) and A. Torralba et al. (2025), integrated with the NIST data base (A. Kramida et al. 2024, shaded regions in Fig. 2). As we find no difference in our fitting results whether these masks are considered or not, we conclude that these lines, if present at all, are so weak that they do not influence our analysis, and are not added to the emission line model. Of these, we only tentatively detect He I λ6678, with a flux that is <1 per cent of narrow Hα.

The fitting results are displayed in Figs 2 and 3; the salient best-fitting parameters used in the discussion are reported in Table 1 and in their entirety in Appendix B. To test for potential biases introduced by the high Hα SNR (SNR = 150 for Hα versus SNR = 25 and 50 for Hβ and Paβ, respectively), we separately fit the Hβ line, which has the lowest SNR and is the most affected by potential faint lines contamination, and check for parameter consistency.

4 DISCUSSION

If the electron scattering scenario were correct, we would expect the following properties to hold for the three hydrogen lines analysed in this Letter:

(i) The widths of the broad Gaussian components should be similar (within 25 per cent; J. E. Greene & L. C. Ho 2005), as they represent recombination or collisionally excited emission from similar regions within the same BLR.

(ii) The exponential widths, W, should be the same for all lines, as electron scattering is wavelength independent over the considered spectral range.

(iii) The observed scattered fractions $f_{\rm scatt}$ should satisfy

$$f_{\rm scatt,Pa\,\beta} \geq f_{\rm scatt,H\,\alpha} \geq f_{\rm scatt,H\,\beta}. \quad (4)$$

The latter inequality accounts for the possible presence of dust in the scattering medium. If dust is present, since scattered light travels through more material than the transmitted counterpart of the same line, it is subject to higher optical depth and is therefore more likely to be absorbed. We thus expect that for each line, the scattered component can be more strongly attenuated than the transmitted component. This effect is stronger for bluer lines, since dust attenuation is stronger at shorter wavelengths. For this reason, dust causes the observed scattered fraction to be lower for bluer lines, even if the intrinsic scattered fraction is the same.

Our baseline (model 1) best-fitting results for FWHM$_{\rm broad}$, W, and $f_{\rm scatt}$ are reported in Table 1 for all three hydrogen lines, and their posterior distributions are shown in Fig. 3. It is clear that none of the three previously mentioned conditions are met, suggesting that the exponential model, although able to successfully reproduce the individual profiles separately, fails in simultaneously reproducing them, at least for this specific LRD. Our $W_{\rm H\,\alpha}$ value is consistent with that obtained from single Hα modelling, and in general with the results from R25, as the exponential widths in their sample vary in the range 1000–2000 km s^{-1}. In contrast, both $W_{\rm H\,\beta}$ and $W_{\rm Pa\,\beta}$ are fundamentally unconstrained. The Gaussian broad components have widths that differ by a factor of >3, and also the scattered fractions are not consistent, nor do they satisfy equation (4), as Paβ is fundamentally unconstrained and exhibits the lowest $f_{\rm scatt}$.

Since our baseline model cannot put satisfactory constraints on $W_{\rm H\,\beta}$ and $W_{\rm Pa\,\beta}$, we further test the electron scattering scenario by performing additional fits satisfying one of conditions (i)–(iii) at a time. First, we enforce the same FWHM$_{\rm broad}$ for the three hydrogen lines, while allowing the exponential parameters to vary freely (model 2). Then, we tie both W and $f_{\rm scatt}$, and leave FWHM$_{\rm broad}$ independent (model 3). The best-fitting parameters for these models are reported in Table 1. We also test a more restrictive model where the broad profiles of the three lines are fully tied, i.e. we force them to have the same FWHM$_{\rm broad}$, W, and $f_{\rm scatt}$ (model 4). Lastly, we compare our set of exponentials with a double-Gaussian model, where broad emission in each line is modelled using two Gaussian components with the same velocity and independent width. For each of our analysed models, both exponential and Gaussian, we report the $\chi^2_{\rm red}$ and BIC of the best fits in Table 2. Model 4 yields the poorest fit, while models 2 and 3 perform well, although neither is able to simultaneously satisfy conditions (i)–(iii). In model 2, Hβ and Paβ exponential profiles differ by a factor of 2–4 with respect to the baseline model, and their scattered fractions saturate at $\sim$1 (Fig. C1), allowing only for a 3σ lower limit estimate. In model 3, broad line widths differ by a factor of >4. The double-Gaussian model performs worse than our exponential models 1–3, likely because the final fit statistic is always dominated by the bright Hα line, which is best reproduced by an exponential profile (Section 3), in agreement with previous findings (R25). Such exponential preference is weaker for Hβ and Paβ, consistent with their small scattered fractions (Table 1). Single-line fits indicate that broad Paβ is better described by a single Gaussian, while Hβ yields no robust parameter constraints due to strong Balmer absorption and the nearby [O III] emission complicating the continuum placement. In summary, our results rule out the simple scenario in which broad lines are scattered by an embedding ionized medium into much more extended exponential wings. Such a model would predict identical exponential widths and scattered fractions (in the absence of dust) for all three hydrogen lines, which we do not observe.

Further evidence against this picture comes from I. Juodžbalis et al. (2025a), who argue that such an ionized medium surrounding the BLR should recombine and therefore emit in Hα, which, however,

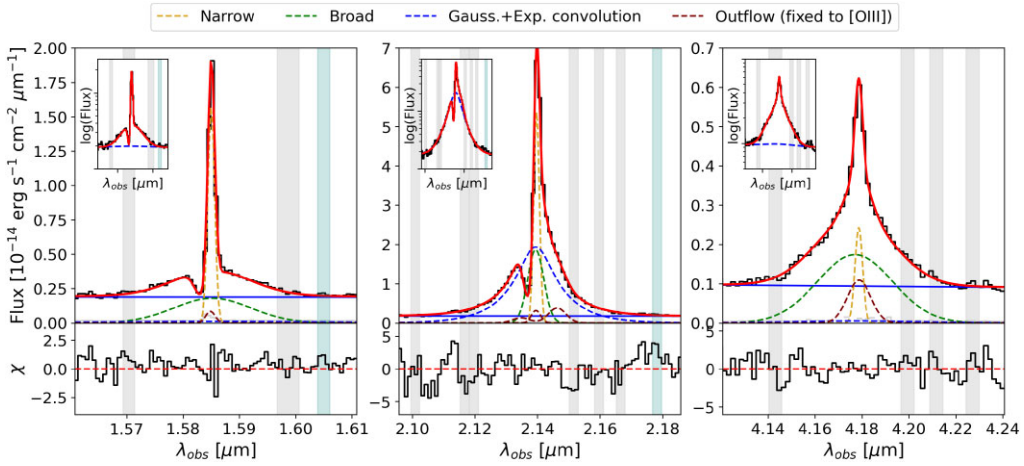

Figure 2. Best-fitting models for H β (left), H α (centre), and Pa β (right). Individual model components are reported in different colours; each line is decomposed into three Gaussians (narrow, outflow, and broad unscattered components) and the exponential convolution representing the broad scattered component. For the H β and H α, the absorber is also modelled. The three inset panels report the line profiles in logarithmic scale, with the best-fitting model in red and the exponential component in blue. Shaded regions indicate the locations of possible He I (light blue) and [Fe II] (light grey) lines.

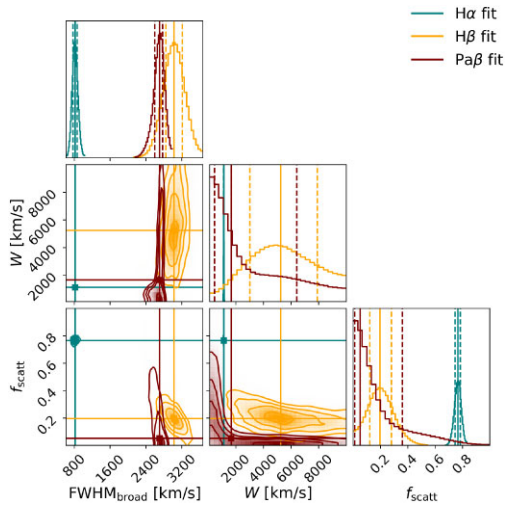

Figure 3. Posterior distributions of FWHM$_{broad}$, W, and f_{scatt} for H α (teal), H β (orange), and Pa β (maroon).

is not detected. In the same work, the authors also rule out the simple Balmer scattering scenario (R. P. Naidu et al. 2025), which would also imply 2 dex smaller black hole masses. In this alternative picture, H α and H β are broadened by resonant Balmer scattering; however, the predicted H α/H β flux ratio is $\sim$100 (S.-J. Chang et al. 2025), far higher than what is observed in the Rosetta Stone, and in most high-redshift LRDs. Moreover, Paschen lines should exhibit narrower profiles, as they are expected to remain largely unaffected by Balmer resonant scattering: instead, contrary to these expectations and consistently with I. Juodžbalis et al. (2024), in our work we find that Pa β has a similar width to H β, and is in fact broader than H α.

If not from an ionized medium embedding the BLR, then what is the origin of the broad line wings observed in many high-redshift AGNs and LRDs? The use of exponential, or Lorentzian, or power-law functional forms (which all differ from the Gaussian profile, but are essentially undistinguishable in the vast majority of spectra) for fitting the broad line wings is not a new proposal – these profiles have been already largely invoked and used in a variety of previous works for fitting local and lower redshift AGNs and quasars (M. P. Véron-Cetty, P. Véron & A. C. Gonçalves 2001; T. Nagao, A. Marconi & R. Maiolino 2006; J. R. Mullaney & M. J. Ward 2008; W. Kollatschny & M. Zetzl 2011; V. Cracco et al. 2016; J. Scholtz et al. 2021). However, in the past, the wings of these lower redshift (and much brighter) AGNs were mainly explained in terms of macroturbulence in the BLR, or strong rotation support, or radiation-pressure-driven winds (J. A. Baldwin 1975; W. Kollatschny & M. Zetzl 2011; M. R. Goad, K. T. Korista & A. J. Ruff 2012). Given our results, these may be simpler explanations that do not imply black hole masses that are two orders of magnitude lower than inferred from the virial relations. Within this context, it is important to note that reverberation mapping of local AGNs that display such broad wings that can be fitted with Lorentzian or exponential profiles, follow the same virial relations established for other AGNs (P. Du & J.-M. Wang 2019). Finally, recently the black hole mass of a prototypical, lensed LRD at $z = 7$ has been measured directly by resolving its sphere of influence, and the black hole mass is found to be fully consistent with the value derived from the virial relations, and about two orders of magnitude higher than inferred by the scattering scenario (I. Juodžbalis et al. 2025b).

5 SUMMARY AND CONCLUSIONS

In this Letter, we have tested the hypothesis that the broad H α emission observed in LRDs is due to electron scattering by an ionized medium embedding the BLR (R25). We have studied the spectral profiles of the H α, H β, and Pa β emission lines in the Rosetta Stone, the brightest known LRD (GN-28074 at $z = 2.26$), by fitting an exponential model with various set-ups to all three lines simultaneously. While the exponential fit to H α alone is excellent, these models fail to reproduce all three line profiles simultaneously while satisfying physically motivated constraints on their shapes and scattered fractions [conditions (i)–(iii), Section 4]. Our findings suggest that the electron scattering scenario is either incomplete, potentially relaxing our conditions (i)–(iii), or outright incorrect. We have also ruled out the simple Balmer scattering scenario, based on the finding that Pa β is broader than H β and has a width similar to H α, as already pointed out by I. Juodžbalis et al. (2024). Together, these results establish the Rosetta Stone as a clear counterexample to

Table 1. Specific line fitting results for the different analysed BLR emission models of H α, H β, and Pa β.

Model	Line	FWHM (km s^{-1})	W (km s^{-1})	$f_{\rm scatt}$
Baseline (model 1)	H α	814^{+49}_{-46}	1120^{+13}_{-13}	$0.766^{+0.018}_{-0.020}$
	H β	3026^{+183}_{-184}	5252^{+2642}_{-2245}	$0.20^{+0.08}_{-0.07}$
	Pa β	2705^{+67}_{-112}	1656^{+4768}_{-1190}	$0.05^{+0.03}_{-0.04}$
W, $f_{\rm scatt}$ free FWHM$_{\rm broad}$ bound (model 2)	H α		1101^{+13}_{-17}	$0.69^{+0.04}_{-0.03}$
	H β	661^{+40}_{-52}	1230^{+40}_{-58}	>0.96
	Pa β		911^{+18}_{-19}	>0.98
W, $f_{\rm scatt}$ bound FWHM$_{\rm broad}$ free (model 3)	H α	699^{+48}_{-47}		
	H β	575^{+59}_{-74}	1090^{+13}_{-13}	$0.75^{+0.03}_{-0.03}$
	Pa β	2381^{+57}_{-57}		

Table 2. Model statistics.

Model	Parameters	$\chi^2_{\rm red}$	BIC
Baseline (model 1)	FWHM$_{\rm broad}$, W, $f_{\rm scatt}$ free	3.03	672
Model 2	W, $f_{\rm scatt}$ free FWHM$_{\rm broad}$ tied	3.71	949
Model 3	FWHM$_{\rm broad}$ free W, $f_{\rm scatt}$ tied	3.13	680
Model 4	FWHM$_{\rm broad}$, W, $f_{\rm scatt}$ tied	4.80	961
Double Gaussian	—	4.59	931

the claim that black hole masses are universally and systematically overestimated due to electron or Balmer scattering effects.

When comparing models, attention should be paid to the disproportionate weight of H α in the SNR distribution. More generally, we underscore the importance of using constraints from multiple lines to robustly investigate the physical processes at play in AGNs. The claim of black hole masses underestimated by two orders of magnitude in LRDs, because of the putative scattering scenario, is therefore not supported by our results on this prototypical, bright LRD.

ACKNOWLEDGEMENTS

We thank V. Rusakov for valuable suggestions that improved the clarity and completeness of this Letter. The research activities described in this Letter were carried out with contribution of the Next Generation EU funds within the National Recovery and Resilience Plan (PNRR), Mission 4 – Education and Research, Component 2 – From Research to Business (M4C2), Investment Line 3.1 – Strengthening and Creation of Research Infrastructures, Project IR0000034 – 'STILES – Strengthening the Italian Leadership in ELT and SKA'. MB, FDE, RM, XJ, JS, IJ, and GCJ acknowledge support by the Science and Technology Facilities Council (STFC), by the ERC through Advanced Grant 695671 'QUENCH', and by the UKRI Frontier Research grant RISEandFALL. RM also acknowledges funding from a research professorship from the Royal Society. IJ also acknowledges support from the Huo Family Foundation through a P. C. Ho PhD Studentship. This Letter is based on observations made with the NASA/ESA/CSA *James Webb Space Telescope*. The data were obtained from the *Mikulski Archive for Space Telescopes* at the Space Telescope Science Institute, which is operated by the Association of Universities for Research in Astronomy, Inc., under NASA contract NAS 5-03127 for *JWST*. These observations are associated with program 1181.

DATA AVAILABILITY

The data used in this Letter are available from the JADES public DR3 (F. D'Eugenio et al. 2025c, Bsemi DOI: 10.17909/8tdj-8n28).

REFERENCES

Baldwin J. A., 1975, ApJ, 201, 26
Bunker A. J. et al., 2024, A&A, 690, A288
Chang S.-J., Gronke M., Matthee J., Mason C., 2025, preprint (arXiv:2508.08768)
Cracco V., Ciroi S., Berton M., Di Mille F., Foschini L., La Mura G., Rafanelli P., 2016, MNRAS, 462, 1256
D'Eugenio F. et al., 2025a, preprint (arXiv:2503.11752)
D'Eugenio F. et al., 2025b, preprint (arXiv:2506.14870)
D'Eugenio F. et al., 2025c, ApJS, 277, 4
Du P., Wang J.-M., 2019, ApJ, 886, 42
Eisenstein D. J. et al., 2023, preprint (arXiv:2306.02465)
Ferruit P. et al., 2022, A&A, 661, A81
Foreman-Mackey D., Hogg D. W., Lang D., Goodman J., 2013, PASP, 125, 306
Furtak L. J. et al., 2025, A&A, 698, A227
Goad M. R., Korista K. T., Ruff A. J., 2012, MNRAS, 426, 3086
Gordon K. D., Clayton G. C., Misselt K. A., Landolt A. U., Wolff M. J., 2003, ApJ, 594, 279
Greene J. E., Ho L. C., 2005, ApJ, 630, 122
Greene J. E. et al., 2024, ApJ, 964, 39
Hainline K. N. et al., 2025, ApJ, 979, 138
Harikane Y. et al., 2023, ApJ, 959, 39
Inayoshi K., Maiolino R., 2025, ApJ, 980, L27
Jakobsen P. et al., 2022, A&A, 661, A80
Ji X. et al., 2025a, MNRAS, in press (arXiv:2501.13082)
Ji X. et al., 2025b, preprint (arXiv:2507.23774)
Juodžbalis I. et al., 2024, MNRAS, 535, 853
Juodžbalis I. et al., 2025a, preprint (arXiv:2504.03551)
Juodžbalis I. et al., 2025b, preprint (arXiv:2508.21748)
Kocevski D. D. et al., 2023, ApJ, 954, L4
Kollatschny W., Zetzl M., 2011, Nature, 470, 366
Kramida A., Ralchenko Y., Reader J., NIST ASD Team, 2024, NIST Atomic Spectra Database (version 5.12). National Institute of Standards and Technology, Gaithersburg, MD. [Online]. Available:https://physics.nist.gov/asd
Labbe I. et al., 2024, preprint (arXiv:2412.04557)
Laor A., 2006, ApJ, 643, 112
Loiacono F. et al., 2025, A&A, 703, A36

Maiolino R. et al., 2024, A&A, 691, A145
Maiolino R. et al., 2025, MNRAS, 538, 1921
Matthee J. et al., 2024, ApJ, 963, 129
Mazzolari G. et al., 2024, preprint (arXiv:2412.04224)
Mazzolari G. et al., 2025, A&A, 700, A12
Mullaney J. R., Ward M. J., 2008, MNRAS, 385, 53
Nagao T., Marconi A., Maiolino R., 2006, A&A, 447, 157
Naidu R. P. et al., 2025, preprint (arXiv:2503.16596)
Planck Collaboration VI, 2020, A&A, 641, A6
Rusakov V. et al., 2025, preprint (arXiv:2503.16595) (R25)
Scholtz J. et al., 2021, MNRAS, 505, 5469
Torralba A. et al., 2025, preprint (arXiv:2510.00103)
Véron-Cetty M. P., Véron P., Gonçalves A. C., 2001, A&A, 372, 730
Wang B. et al., 2025, ApJ, 984, 121
Zhang Z., Jiang L., Liu W., Ho L. C., Inayoshi K., 2025, preprint (arXiv:2506.04350)

APPENDIX A: OXYGEN LINE FITTING AND OUTFLOW CHARACTERIZATION

Before analysing the hydrogen lines, we first fit the [O III] λλ4959, 5007 doublet separately to identify and, if present, constrain the outflow properties. The fitting procedure follows the approach described in Section 3. Each [O III] line is modelled with a narrow and a two-Gaussian outflow component. The two outflow line widths are allowed to vary, respectively, in the ranges 100–900 km s^{-1} and 900–10 000 km s^{-1}, and are constrained to have the same velocity. Our fitting results are shown in the upper panel of Fig. A1.

The need for a double-Gaussian outflow model is motivated by the fact that a single-Gaussian outflow model would result in a poor fit, particularly around the brighter [O III] 5007 line. This is illustrated in the lower panel of Fig. A1, where the residuals from the single- and double-Gaussian fits are shown in grey and black, respectively. The double-Gaussian outflow model is statistically preferred, with a ΔBIC of 134. The two outflow components exhibit a velocity of $v_{\rm out} = -142 \pm 3$ km s^{-1}, and have widths of FWHM$_{\rm out,1} = 317 \pm 26$ km s^{-1} and FWHM$_{\rm out,2} = 1654^{+150}_{-202}$ km s^{-1}. The corresponding line fluxes are summarized in Table A1. Given that the broader outflow component contributes less than 10 per cent of the total outflow flux, in the hydrogen line fitting, we adopt the width of the narrower outflow component only.

We also attempt an exponential fit of the [O III] lines, using the same exponential model described in Section 3. This fit yields to a low values of the scattered fraction ($f_{\rm scatt,[O\,III]} \sim 0.1$) and exponential width ($W_{\rm [O\,III]} \sim 490$ km s^{-1}), suggesting that oxygen may experience electron scattering only in the outer, lower density regions of the gas envelope, where oxygen can recombine. However, this exponential model does not include an outflow component for [O III] – and therefore also for the hydrogen lines – which is instead necessary for accurately reproducing the latter. For this reason, we keep the double-Gaussian model as our fiducial outflow description.

Table A1. Line fluxes for the [O III] narrow and outflow components, resulting from our double-Gaussian outflow model. They are not dust-corrected.

Line	Flux (10^{-18} erg s^{-1} cm^{-2})
[O III]$_{\rm narrow}$	80^{+12}_{-10}
[O III]$_{\rm out,1}$	63^{+9}_{-11}
[O III]$_{\rm out,2}$	13^{+1}_{-1}

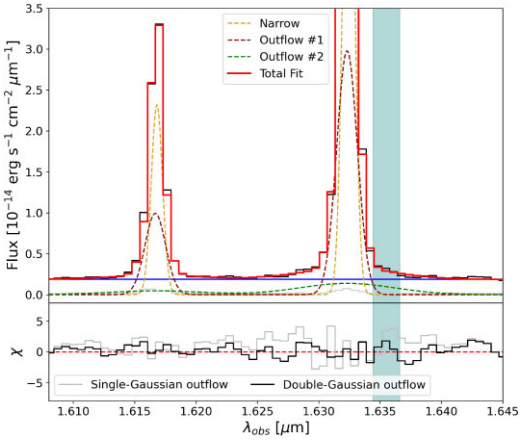

Figure A1. Fit of [O III] λλ4959, 5007 doublet. Each line is modelled with a narrow and a double-Gaussian outflow component. In the lower panel, we compare the residuals of the fit with the single-Gaussian outflow model to highlight the inadequacy of the latter in correctly reproducing oxygen emission. The shaded region indicates the location of the He I λ5017 line.

A more in-depth analysis of outflow properties of GN-28074 is beyond the scope of this work, but will be addressed in future research.

APPENDIX B: COMPLETE FITTING RESULTS FOR THE BASELINE EXPONENTIAL MODEL

In Table B1, we provide the flux list for all measured hydrogen emission line components: narrow, broad unscattered, broad scattered, and outflow. The intrinsic narrow FWHM is 89 ± 3 km s^{-1}, and is the same for the three hydrogen lines, as well as for the [N II] λλ6548, 6584 doublet, which is tentatively detected at 4σ confidence. We estimate dust extinction for each component of our model from the Hα/Hβ flux ratio, by assuming a standard case B decrement of 2.86 and the Small Magellanic Cloud extinction curve from K. D. Gordon et al. (2003). We obtain $A_V = 1.22^{+0.24}_{-0.18}$ for the narrow,

Table B1. Line fluxes resulting from our baseline model fitting procedure. They are not dust-corrected.

Line	Flux (10^{-18} erg s^{-1} cm^{-2})
H $\beta_{\rm narrow}$	24^{+1}_{-2}
H $\beta_{\rm broad,unscatt}$	31^{+3}_{-3}
H $\beta_{\rm broad,scatt}$	7^{+3}_{-3}
H $\beta_{\rm outflow}$	<3
H $\alpha_{\rm narrow}$	121^{+8}_{-8}
H $\alpha_{\rm broad,unscatt}$	119^{+10}_{-9}
H $\alpha_{\rm broad,scatt}$	393^{+10}_{-14}
H $\alpha_{\rm outflow}$	11^{+9}_{-7}
[N II] λ6584	27^{+2}_{-3}
Pa $\beta_{\rm narrow}$	10^{+1}_{-1}
Pa $\beta_{\rm broad,unscatt}$	70^{+3}_{-8}
Pa $\beta_{\rm broad,scatt}$	<5
Pa $\beta_{\rm outflow}$	14^{+1}_{-1}

Table B2. Properties of Balmer absorbers, assuming the same covering fraction, velocity shift, and dispersion.

Absorption parameter	Value
C_f	$0.96^{+0.03}_{-0.04}$
$\tau_{0,H\alpha}$	$2.36^{+0.29}_{-0.21}$
$\tau_{0,H\beta}$	$0.83^{+0.11}_{-0.11}$
Δv_{abs} (km s^{-1})	-409^{+20}_{-20}
FWHM$_{abs}$ (km s^{-1})	567^{+24}_{-25}

$A_V = 1.05^{+0.30}_{-0.39}$ for the broad unscattered, and $A_V = 5.73^{+1.00}_{-0.31}$ for the broad scattered components, respectively. Given that for the H β outflow component our fit provides only an upper limit, we estimate $A_{V,\mathrm{outflow}} > 3$.

In Table B2, we report the properties of H α and H β absorbers. The retrieved covering fraction of 0.98 suggests that the dense medium is almost entirely covering the BLR. Our optical depth estimates differ from those retrieved in I. Juodžbalis et al. (2024) because of the different BLR emission model. The differences in Δv_{abs} and σv_{abs} can be attributed to the presence of degeneracies between emission and absorption parameters.

APPENDIX C: POSTERIOR DISTRIBUTIONS OF EXPONENTIAL PARAMETERS FOR MODELS 2 AND 3

Fig. C1 displays the posterior distributions of FWHM$_{broad}$, W, and f_{scatt} from model 2 (broad widths bound, exponential parameters free) and model 3 (broad widths free, exponential parameters bound).

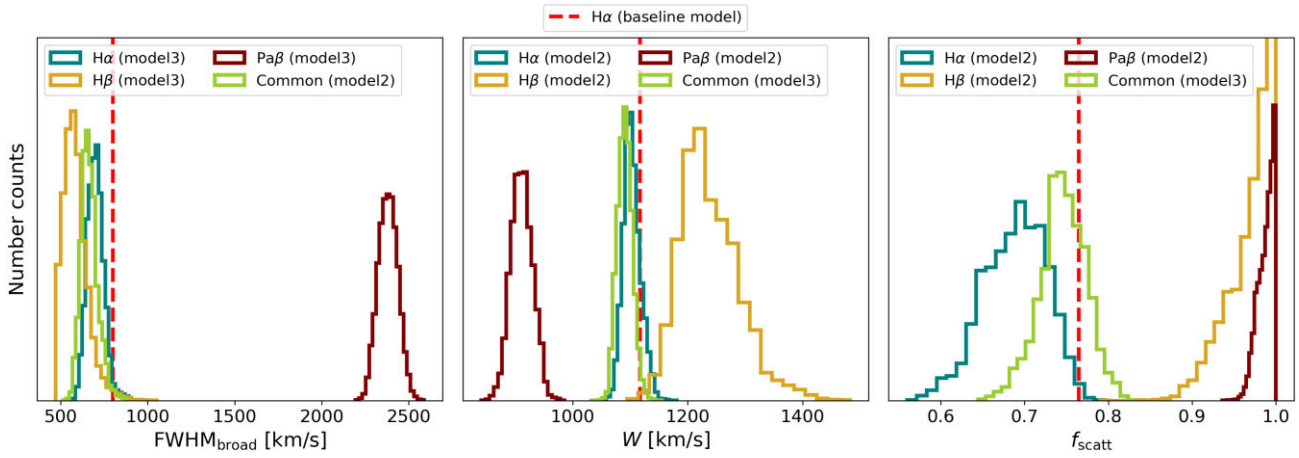

Figure C1. Posterior distributions of FWHM$_{broad}$, W, and f_{scatt} from models 2 and 3. In model 2, the three line widths are bound and the exponential parameters are free to vary, while in model 3, it is the opposite. Common parameters are displayed in green, while single-line parameters are displayed in teal for H α, gold for H β, and maroon for Pa β.

This paper has been typeset from a TEX/LATEX file prepared by the author.